Journal of Fluorescence, Vol. 9, No. 3, 1999

Structural Transition in the Micellar Assembly: A Fluorescence Study

Satinder S. Rawat[1] and Amitabha Chattopadhyay[1,2]

Received September 30, 1998; accepted December 16, 1998

Structural transition can be induced in charged micelles by increasing the ionic strength of the medium. Thus, spherical micelles of sodium dodecyl sulfate (SDS) that exist in water at concentrations higher than the critical micelle concentration assume an elongated rod-like structure in the presence of an increased electrolyte concentration. This is known as sphere-to-rod transition. In this paper, we characterize the change in organization and dynamics that is accompanied by the salt-induced sphere-to-rod transition in SDS micelles using wavelength-selective fluorescence and other steady-state and time-resolved fluorescence parameters. Since the change in micelle organization during such structural transition may not be limited to one region of the micelle, we have selectively introduced fluorophores in two distinct regions of the micelle. We used two probes, *N*-(7-nitrobenz-2-oxa-1,3-diazol-4-yl)-1,2-dipalmitoyl-*sn*-glycero-3-phosphoethanolamine (NBD-PE) and 25-[*N*-[(7-nitrobenz-2-oxa-1,3-diazol-4-yl)-methyl]amino]-27-norcholesterol (NBD-cholesterol), for monitoring the two regions of the micelle. NBD-PE monitors the interfacial region of the micellar assembly, while NBD-cholesterol acts as a reporter for the deeper regions of the micellar interior. Our results show that wavelength-selective fluorescence, in combination with other fluorescence parameters, offers a powerful way to monitor structural transitions induced in charged micelles. These results could be significant to changes in membrane morphology observed under certain physiological conditions.

KEY WORDS: Structural transition; wavelength-selective fluorescence; red edge excitation shift; sodium dodecyl sulfate micelles; salt.

INTRODUCTION

Detergents are extremely important in studies of biological membranes due to their ability to solubilize membrane proteins and receptors [1–6]. They are soluble amphiphiles and, above a critical concentration (strictly speaking, a narrow concentration range), known as the critical micelle concentration (CMC), self-associate to form thermodynamically stable, noncovalent aggregates called micelles [7]. Studies on micellar organization and dynamics assume special significance in light of the fact that the general principles underlying the formation of micelles are common to other related assemblies such as reverse micelles, bilayers, liposomes, and biological membranes [7–10]. Micelles have been used as membrane mimetics to characterize membrane proteins and peptides [11–14]. Micelles offer certain inherent advantages in spectroscopic studies over membranes since micelles are smaller and optically transparent, have well-defined sizes, and are relatively scatter-free. Further, micelles can be of any desired charge type and can adopt different shapes and internal packing, depending on the chemical structures of the constituent monomers and the ionic strength of the medium [15–17].

Micelles are highly cooperative, organized molecular assemblies of amphiphiles and are dynamic in nature [18,19]. The organization and dynamics of micellar envi-

[1] Centre for Cellular and Molecular Biology, Uppal Road, Hyderabad 500 007, India.

[2] To whom correspondence should be addressed. Fax: +91-40-7171195. e-mail: amit@ccmb.ap.nic.in

1053-0509/99/0900-0233$16.00/0

ronments, namely, the core, the interface, and the immediate layers of water on the interface, have been investigated using experimental [20–28] and theoretical [29,30] approaches. It is fairly well established now that practically all types of molecules have a surface-seeking tendency in micelles (due to very large surface area-to-volume ratio) and that the interfacial region is the preferred site for solubilization, even for hydrophobic molecules [22,31–33].

Structural transition can be induced in charged micelles at a given temperature by increasing the ionic strength of the medium or amphiphile concentration [15–17,34–38]. Thus, spherical micelles of sodium dodecyl sulfate (SDS) that exist in water at concentrations higher than the CMC assume an elongated rod-like structure in the presence of an increased electrolyte (salt) concentration when interactions among the charged headgroups are attenuated due to the added salt (see Fig. 1). This is known as sphere-to-rod transition [36]. This shape change induced by increased salt concentrations is accompanied by a reduction in the CMC [39–41]. It has been suggested that large rod-shaped micelles are better models for biomembranes [34] and the hydrocarbon chains are more ordered in rod-shaped micelles compared to spherical micelles [42], giving rise to a higher microviscosity in rod-shaped micelles [43].

A direct consequence of any organized molecular assembly (such as membranes or micelles) is the restriction imposed on the dynamics and mobility of the constituent structural units. We have previously shown that the microenvironment of molecules bound to such organized assemblies can be conveniently monitored using wavelength-selective fluorescence as a novel tool [28,44–51]. Wavelength-selective fluorescence comprises a set of approaches based on the red edge effect in fluorescence spectroscopy which can be used to monitor directly the environment and dynamics around a fluorophore in a complex biological system [52]. A shift in the wavelength of maximum fluorescence emission toward higher wavelengths, caused by a shift in the excitation wavelength toward the red edge of the absorption band, is termed the red edge excitation shift (REES). This effect is mostly observed with polar fluorophores in motionally restricted media such as very viscous solutions or condensed phases [52,53, and references therein]. This phenomenon arises from the slow rates of solvent relaxation (reorientation) around an excited state fluorophore, which is a function of the motional restriction imposed on the solvent molecules in the immediate vicinity of the fluorophore. By utilizing this approach, it becomes possible to probe the mobility parameters of the environment itself (which is represented by the relaxing solvent molecules) using the fluorophore merely as a reporter group. Further, since the ubiquitous solvent for biological systems is water, the information obtained in such cases will come from the otherwise "optically silent" water molecules. This makes REES and related techniques extremely useful in biology since hydration plays a crucial modulatory role in a large number of important cellular events [54] such as lipid–protein interactions [55] and ion transport [56–58].

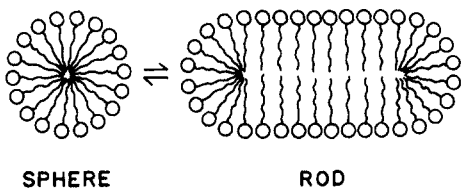

Fig. 1. A schematic representation of the sphere-to-rod transition in charged SDS micelles induced by salt. Note that the headgroup spacing is reduced in rod-shaped micelles due to attenuation of interactions among the charged headgroups by the added salt.

We have shown earlier that REES and related techniques (wavelength-selective fluorescence approach) serve as a powerful tool to monitor organization and dynamics of membrane-bound probes and peptides [44–47,50,51]. We have recently extended the application of this approach to micellar systems. We demonstrated, using the widely used probe *N*-(7-nitrobenz-2-oxa-1,3-diazol-4-yl)-1,2-dipalmitoyl-*sn*-glycero-3-phosphoethanolamine (NBD-PE), the usefulness of this approach for examining the organization and dynamics of a variety of micelles differing in charge and shape [28]. Wavelength-selective fluorescence thus represents a powerful tool for studying micellar organization and dynamics.

In this paper, we have characterized the change in organization and dynamics that is accompanied by the salt-induced sphere-to-rod transition in sodium dodecyl sulfate (SDS) micelles using wavelength-selective fluorescence and other steady-state and time-resolved fluorescence parameters. Since the change in micelle organization during such structural transition may not be limited to a particular region of the micelle, but may affect the total morphology of the micellar assembly, we have selectively introduced fluorophores in two distinct regions (the interfacial and the deeper hydrocarbon regions) of the micelle. For this purpose, we have employed two probes, NBD-PE and 25-[*N*-[(7-nitrobenz-2-oxa-1,3-diazol-4-yl)-methyl]amino]-27-norcholesterol (NBD-cholesterol), for monitoring two regions of the micelle (see Fig. 2). 7-Nitrobenz-2-oxa-1,3-diazol-4-yl (NBD)-labeled lipids are widely used as fluorescent analogues of native lipids in micelles and in biological and model membranes to study a variety of processes [59,60]. In NBD-PE, the NBD group is covalently attached to the

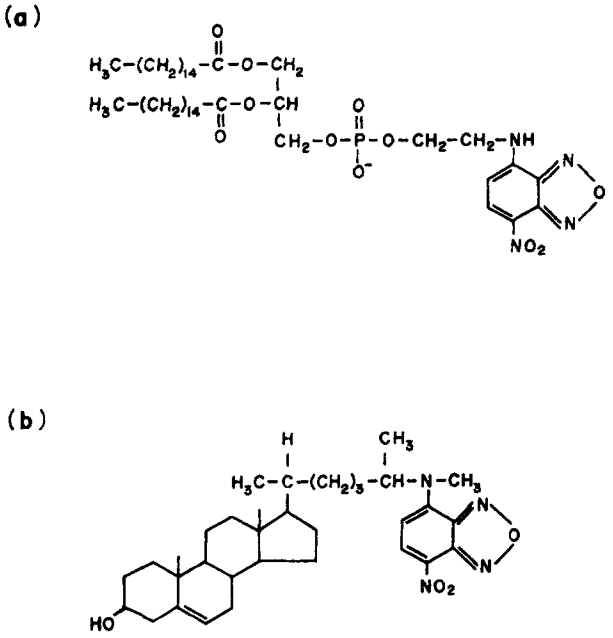

Fig. 2. Chemical structures of (a) NBD-PE and (b) NBD-cholesterol.

headgroup of a phosphatidylethanolamine molecule. The NBD group in NBD-PE has been shown to be localized in the interfacial region of the membrane [61–66] and its location in the micellar environment is most likely to be interfacial. In contrast to this, the NBD group in NBD-cholesterol is attached to the flexible acyl chain of the cholesterol molecule (Fig. 2). The NBD group of this molecule has been found to be localized deep in the hydrocarbon region of the membrane [61,62,67], and likewise, its location in micellar systems would be deep inside the micellar core.

EXPERIMENTAL

Materials. SDS, cobalt chloride, and sodium chloride were purchased from Sigma Chemical Co. (St. Louis, MO). NBD-PE, NBD-cholesterol, and 1,6-diphenyl-1,3,5-hexatriene (DPH) were obtained from Molecular Probes (Eugene, OR). Dioleoyl-*sn*-glycero-3-phosphocholine (DOPC) was from Avanti Polar Lipids (Birmingham, AL). All other chemicals used were of the highest purity available. Solvents used were of spectroscopic grade. Water was purified through a Millipore (Bedford, MA) Milli-Q system and used throughout. The purity of DOPC, NBD-PE, and NBD-cholesterol was checked by thin-layer chromatography on silica gel precoated plates in chloroform/methanol/water (65:35:5, v/v/v, for DOPC and NBD-PE, and 65:35:4, v/v/v, for NBD-cholesterol). DOPC gave only one spot with a phosphate-sensitive spray and subsequent charring [68]. NBD-PE and NBD-cholesterol were found to be pure when detected by their color or fluorescence. The concentration of DOPC was determined by phosphate assay subsequent to total digestion by perchloric acid [69]. Dimyristoyl-*sn*-glycero-3-phosphocholine (DMPC) was used as an internal standard to assess lipid digestion. The purity of SDS was checked by measuring its CMC and comparing it with the literature CMC. The CMC of SDS was determined fluorimetrically using a method previously developed by one of us [41] which utilizes enhancement of DPH fluorescence upon micellization. All experiments were done at room temperature (25°C).

Methods. The concentration of SDS used was 16 m*M*, which is double the CMC of SDS. This was done to ensure that SDS is in the micellar state. The molar ratio of fluorophore to detergent was carefully chosen to give the optimum signal-to-noise ratio with minimal perturbation to the micellar organization and negligible interprobe interactions. The ratio used was 1:10,000 (mol/mol). To incorporate probe (NBD-PE or NBD-cholesterol) into micelles, a small aliquot containing 3.2 nmol of probe (from a stock methanolic solution) was added to the preformed micelles (containing varying amounts of NaCl) in a total volume of 2 ml and mixed well by vortexing for 3 min. Background samples were prepared in the same way except that probe was not added to them. Samples were equilibrated in the dark overnight before measuring fluorescence.

For quenching studies with Co^{2+} ions, small unilamellar vesicles (SUVs) of DOPC containing 1% (mol/mol) of NBD-PE or NBD-cholesterol were used. These vesicles were made by mixing 188 nmol of DOPC in methanol with 1.88 nmol of the probe (NBD-PE or NBD-cholesterol) in methanol. A few drops of chloroform were added and mixed well, and the samples were dried under a stream of nitrogen while being warmed gently (~35°C). After further drying under a high vacuum for at least 3 h, the dried film was swollen by the addition of 1.5 ml of 10 m*M* 3-(*N*-morpholino)propanesulfonic acid (MOPS) and 150 m*M* NaCl, pH 7.2, buffer and vortexed for 3 min to disperse the lipid. The lipid dispersion was sonicated until they were clear (7–10 min, while being cooled in ice) using a Branson Model 250 sonifier fitted with a microtip. The sonicated samples were centrifuged at 12,000 rpm for 10 min to remove any titanium particle shed from the microtip during sonication. Background samples were prepared in the same way except that probe was not added to them. Samples were equilibrated in the dark overnight before measuring fluorescence.

Steady-State Fluorescence Measurements. Steady-state fluorescence measurements were performed with a Hitachi F-4010 spectrofluorometer using 1-cm-path length quartz cuvettes. Excitation and emission slits with a nominal bandpass of 5 nm were used for all measurements. Background intensities of samples in which fluorophores were omitted were negligible in most cases and were subtracted from each sample spectrum to cancel out any contribution due to the solvent Raman peak and other scattering artifacts.

Fluorescence polarization measurements were performed using an Hitachi polarization accessory. Polarization values were calculated from the equation [70]

$$P = \frac{I_{VV} - GI_{VH}}{I_{VV} + GI_{VH}} \tag{1}$$

where I_{VV} and I_{VH} are the measured fluorescence intensities (after appropriate background subtraction) with the excitation polarizer oriented vertically and the emission polarizer oriented vertically and horizontally, respectively. G is the grating correction factor and is equal to I_{HV}/I_{HH}. All experiments were done with multiple sets of samples and average values of polarization are shown in the figures. The spectral shifts obtained with different sets of samples were identical in most cases. In other cases, the values were within ± 1 nm of the ones reported.

For quenching experiments using Co^{2+}, the fluorescence intensities were corrected for inner filter effect using the following equation [71]:

$$F_{correct} = F_{apparent} \times 10^{(A_{ex}+A_{em})/2} \tag{2}$$

where A_{ex} and A_{em} are the measured absorbance at the excitation and emission wavelengths, respectively. The absorbances of the samples were measured using an Hitachi U-2000 UV-visible absorption spectrophotometer after appropriate background subtraction. Quartz cuvettes with a path length of 1 cm were used.

Time-Resolved Fluorescence Measurements. Fluorescence lifetimes were calculated from time-resolved fluorescence intensity decays using a Photon Technology International (London, Western Ontario, Canada) LS-100 luminescence spectrophotometer in the time-correlated single-photon counting mode. This machine uses a thyratron-gated nanosecond flash lamp filled with nitrogen as the plasma gas (17 ± 1 in. of mercury vacuum) and is run at 22–25 kHz. Lamp profiles were measured at the excitation wavelength using Ludox (colloidal silica) as the scatterer. To optimize the signal-to-noise ratio, 5000 photon counts were collected in the peak channel. All experiments were performed using slits with a nominal bandpass of 10 nm. The sample and the scatterer were alternated after every 10% acquisition to ensure compensation for shape and timing drifts occurring during the period of data collection. The data stored in a multichannel analyzer were routinely transferred to an IBM PC for analysis. Intensity decay curves so obtained were fitted as a sum of exponential terms:

$$F(t) = \sum_i \alpha_i \exp(-t/\tau_i) \tag{3}$$

where α_i is a preexponential factor representing the fractional contribution to the time-resolved decay of the component with a lifetime τ_i. The decay parameters were recovered using a nonlinear least-squares iterative fitting procedure based on the Marquardt algorithm [72]. The program also includes statistical and plotting subroutine packages [73]. The goodness of the fit of a given set of observed data and the chosen function was evaluated by the reduced χ^2 ratio, the weighted residuals [74], and the autocorrelation function of the weighted residuals [75]. A fit was considered acceptable when plots of the weighted residuals and the autocorrelation function showed random deviation about zero with a minimum χ^2 value (generally not more than 1.2). To avoid instrumental artifacts, perylene was used as a standard fluorophore, and its fluorescence decay was measured under identical conditions and computational procedures. Mean (average) lifetimes $\langle\tau\rangle$ for biexponential decays of fluorescence were calculated from the decay times and preexponential factors using the following equation [71]:

$$\langle\tau\rangle = \frac{\alpha_1\tau_1^2 + \alpha_2\tau_2^2}{\alpha_1\tau_1 + \alpha_2\tau_2} \tag{4}$$

Global Analysis of Lifetimes. The primary goal of the nonlinear least-squares (discrete) analysis of fluorescence intensity decays discussed above is to obtain an accurate and unbiased representation of a single fluorescence decay curve in terms of a set of parameters (*i.e.*, α_i, τ_i). However, this method of analysis does not take advantage of the intrinsic relations that may exist between the individual decay curves obtained under different conditions. A condition in this context refers to temperature, pressure, solvent composition, ionic strength, pH, excitation/emission wavelength, or any other independent variable which can be experimentally manipulated. This advantage can be derived if multiple fluorescence decay curves, acquired under different conditions, are simultaneously analyzed. This is known as the global analysis in which the simultaneous analyses of multiple decay curves are carried out in terms of internally consistent sets of fitting parameters, thereby enhancing the accuracy of the recovered parameters [76–79]. Global analysis thus turns out to be very useful for the prediction of the manner in which the parameters recovered from a set of separate

fluorescence decays vary as a function of an independent variable and helps distinguish between models proposed to describe a system.

In this paper, we have obtained fluorescence decays as a function of increasing salt concentration. The global analysis, in this case, assumes that the lifetimes are linked among the data files (*i. e.*, the lifetimes for any given component are the same for all decays) but that the corresponding preexponentials are free to vary. This is accomplished by using a matrix mapping of the fitting parameters in which the preexponentials are unique for each decay curve while the lifetimes are mapped out to the same value for each decay. All data files are simultaneously analyzed by the least-squares data analysis method using the Marquardt algorithm (as described above) utilizing the map to substitute parameters appropriately while minimizing the global χ^2. The software used for the global analysis was obtained from Photon Technology International (London, Western Ontario, Canada).

RESULTS

Red Edge Excitation Shift (REES) of Micelle-Bound NBD Probes

We have previously reported the emission maximum of NBD-PE in spherical SDS micelles to be 532 nm in the absence of any added salt [28]. We further reported that as the excitation wavelength was gradually changed from 465 to 520 nm, the emission maxima of NBD-PE bound to spherical SDS micelles shifted from 532 to 542 nm, which corresponds to a REES of 10 nm [28]. The emission maximum of NBD-PE did not show any change and was found to be at 532 nm (when excited at 465 nm) when it was incorporated in rod-shaped SDS micelles present in 0.5 *M* NaCl, suggesting that the NBD group in NBD-PE is localized at the interfacial region of the micelles (Fig. 3). It should be mentioned here that the emission maximum of NBD-PE in model membranes of DOPC, in which the NBD group has been shown to be interfacial [61–66], has been reported to be around 530 nm [45,62]. The shift in the maxima of fluorescence emission[3] of NBD-PE as a function of excitation wavelength, when bound to rod-shaped micelles of SDS containing 0.5 *M* NaCl, is shown in Fig. 3. As the excitation wavelength is changed from 465 to 520 nm, the emission maxima of micelle-bound NBD-PE are shifted from 532 to 542 nm, which corresponds to a REES of 10 nm (Fig. 3). Such dependence of the emission spectra on the excitation wavelength is characteristic of the red edge effect. Observation of this effect in rod shaped micelles implies that the NBD group of NBD-PE, when incorporated in these micelles, is in an environment where its mobility is considerably reduced. Since the NBD group in NBD-PE is localized in the micellar interfacial region, such a result would directly imply that this region of the micelle offers considerable restriction to the reorientational motion of the solvent dipoles around the excited state fluorophore.

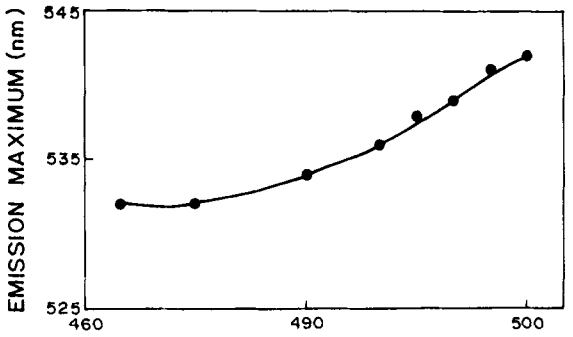

Fig. 3. Effect of changing the excitation wavelength on the wavelength of maximum emission for NBD-PE in micelles of SDS containing 0.5 *M* NaCl. The ratio of NBD-PE to SDS was 1:10,000 (mol/mol). See Experimental for other details.

The above results show that the organizational change brought about by the sphere-to-rod transition could not be detected by REES of the interfacial probe, NBD-PE, since the magnitude of REES was same in both cases, *i.e.*, 10 nm. Since such changes in organization induced by the sphere-to-rod transition could be significant in the inner regions of the micelle, REES of micelle-bound NBD-cholesterol, a deep probe, was examined with varying amounts of salt added. This probe is expected to localize in the deeper region of the micelles (also see results from Co^{2+} quenching experiments discussed below).

The emission maximum of the NBD group is sensitive to the polarity of the probe microenvironment [48,80,81]. When excited at 465 nm, NBD-cholesterol exhibits an emission maximum of 533 nm in spherical micelles of SDS without any added salt (see Fig. 4a). Upon increasing the ionic strength of the medium by gradual addition of NaCl, a progressive blue shift in the emission maxima of the micelle-bound NBD-cholesterol

[3] We have used the term maximum of fluorescence emission in a somewhat wider sense here. In every case, we have monitored the wavelength corresponding to maximum fluorescence intensity, as well as the center of mass of the fluorescence emission. In most cases, both these methods yielded the same wavelength. In cases where minor discrepancies were found, the center of mass of emission has been reported as the fluorescence maximum.

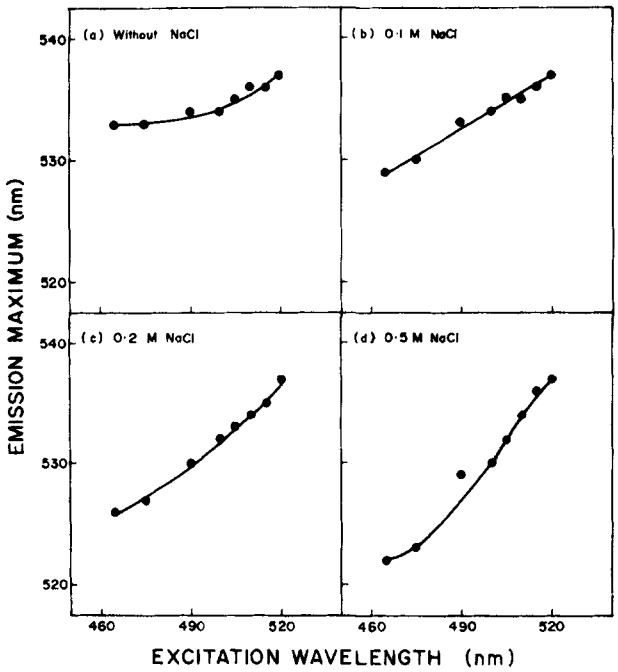

Fig. 4. Effect of changing the excitation wavelength on the wavelength of maximum emission for NBD-cholesterol in SDS micelles containing (a) no, (b) 0.1 *M*, (c) 0.2 *M*, and (d) 0.5 *M* NaCl. The ratio of NBD-cholesterol to SDS was 1:10,000 (mol/mol). See Experimental for other details.

was observed. Thus, the fluorescence emission maxima shifted from 533 nm in the absence of NaCl to 529, 526, and 522 nm in the presence of 0.1, 0.2, and 0.5 *M* NaCl, respectively (see Figs. 4a–d). This indicates a reduction in polarity of the NBD environment with increasing ionic strength, possibly because of a decrease in water content and/or deeper localization of the probe in the micelle. It is interesting to note here that the maximum of emission for NBD-cholesterol incorporated in DOPC vesicles (membranes) is 522 nm [67]. Thus, the emission maximum of NBD-cholesterol in rod-shaped micelles of SDS in 0.5 *M* NaCl approaches that observed in bilayers. This blue shift in emission maxima was accompanied by an approximately twofold increase in the fluorescence intensity of NBD-cholesterol when the NaCl concentration was increased from 0 to 0.5 *M*, indicating a change in the immediate environment experienced by NBD-cholesterol upon sphere-to-rod transition.

This is also apparent from a comparison of REES exhibited by NBD-cholesterol under these conditions. Figures 4a–d show the shifts in the maxima of fluorescence emission of NBD-cholesterol when bound to micelles of SDS as a function of excitation wavelength, with increasing concentrations of NaCl. A significant change in the magnitude of REES was observed upon increasing the ionic strength of the medium. A red shift in the emission maxima of NBD-cholesterol was observed in all cases upon excitation at longer wavelengths. Thus, as the excitation wavelength was changed from 465 to 520 nm, the emission maxima of micelle-bound NBD-cholesterol were shifted from 533 to 537 nm (without NaCl), 529 to 537 nm (in the presence of 0.1 *M* NaCl), 526 to 537 nm (0.2 *M* NaCl), and 522 to 537 nm (0.5 *M* NaCl). This correspond to a REES of 4 nm (in the absence of NaCl), 8 nm (in the presence of 0.1 *M* NaCl), 11 nm (0.2 *M* NaCl) and 15 nm (0.5 *M* NaCl). This clearly indicates differences in microenvironments and packing experienced by the probe in these cases.

Figure 5 shows the fluorescence excitation spectra of NBD-cholesterol incorporated into SDS micelles in the absence and presence of 0.5 *M* NaCl. The excitation maximum in spherical SDS micelles is found to be around 500 nm. Upon the addition of 0.5 *M* NaCl, the excitation maximum shifted from 500 to 479 nm, which is closer

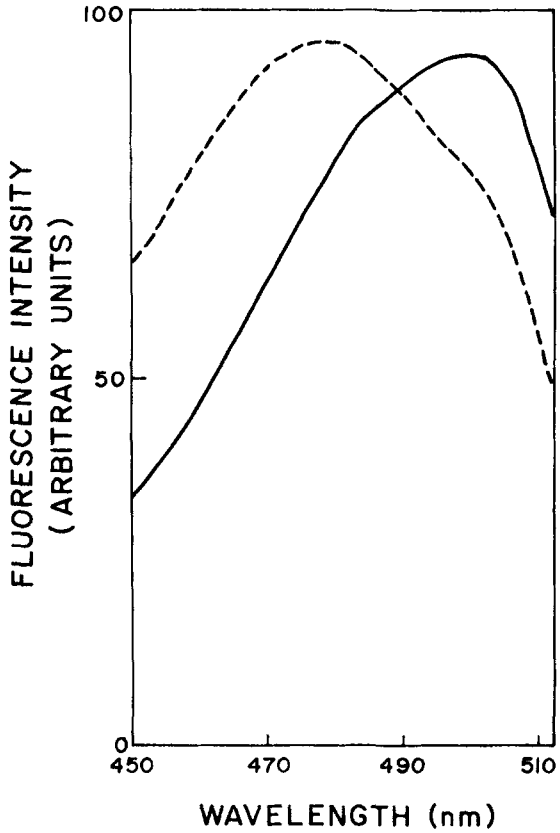

Fig. 5. Fluorescence excitation spectra of NBD-cholesterol in SDS micelles in the absence (——) and in the presence (----) of 0.5 *M* NaCl. The emission wavelength was 530 nm in the absence and 522 nm in the presence of 0.5 *M* NaCl. The spectra are intensity-normalized at the respective excitation maximum. The ratio of NBD-cholesterol to SDS was 1:10,000 (mol/mol). See Experimental for other details.

to the excitation maximum of NBD-cholesterol when incorporated in membranes (data not shown). The excitation spectrum obtained with 0.5 *M* NaCl, however, has a shoulder around 500 nm, possibly indicating the presence of a small population of micelles which did not undergo the sphere-to-rod transition. It is also worthwhile mentioning here that the excitation spectra of NBD-cholesterol obtained with intermediate concentrations of NaCl, between 0 and 0.5 *M*, were broader than the spectra obtained in the absence or presence of 0.5 *M* NaCl. This suggests the presence of different populations of micelles in these samples giving rise to heterogeneity. These results are presented more quantitatively in Fig. 6, where the ratio of fluorescence intensities at 479 and 500 nm is plotted as a function of the NaCl concentration. Figure 6 shows that the ratio increases steadily with increasing concentrations of NaCl, implying that the population of fluorophores with excitation maximum of 479 nm steadily increases with increases in salt concentration. This may be interpreted as additional evidence that the population with excitation maximum at 479 nm is that of the rod-shaped micelles.

Polarization Changes as a Function of NaCl Concentration

Figure 7 shows the change in fluorescence polarization of NBD-PE and NBD-cholesterol in SDS micelles as a function of NaCl concentration. The polarization of micelle-bound NBD-PE shows a steady increase with increasing salt concentrations. This is indicative of tighter packing of the headgroups in rod-shaped micelles (see Fig.1). NBD-PE, which is an interfacial probe, is sensitive

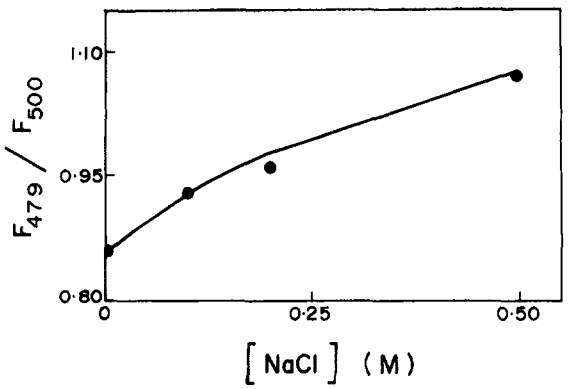

Fig. 6. Change in the ratio of fluorescence intensities of NBD-cholesterol in SDS micelles at excitation wavelengths of 479 and 500 nm as a function of the NaCl concentration. The emission wavelength was fixed at 527 nm. The ratio of NBD-cholesterol to SDS was 1:10,000 (mol/mol). See Experimental for other details.

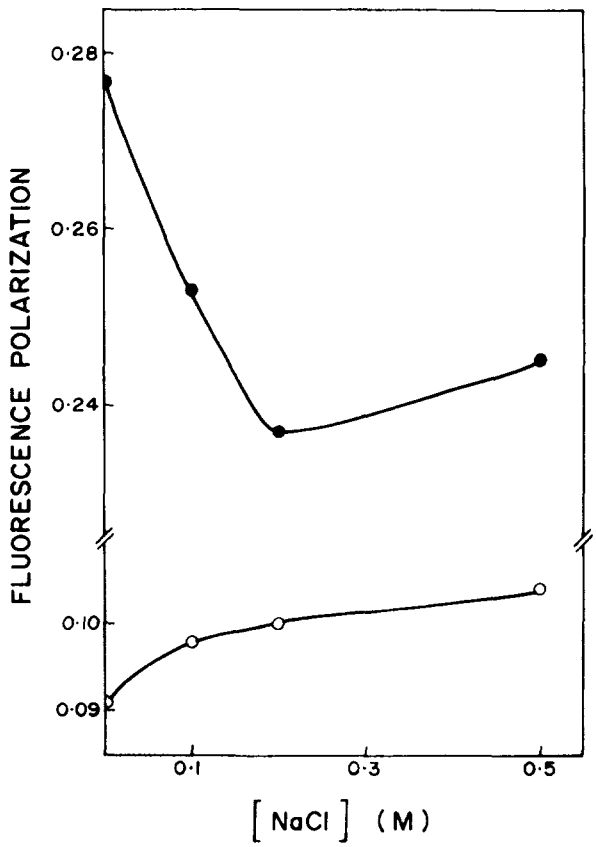

Fig. 7. Fluorescence polarization of NBD-PE (○) and NBD-cholesterol (●) in SDS micelles as a function of NaCl concentration. Excitation was at 465 nm and polarization values were recorded at 535 nm. The ratio of probe to SDS was 1:10,000 (mol/mol). See Experimental for other details.

to the difference in packing caused by the sphere-to-rod transition induced by NaCl, and this gives rise to the increase in polarization. It should be noted here that the polarization values are in general higher in electrically neutral micelles (such as Triton X-100 and CHAPS), in which packing of headgroups is tighter, compared to those in charged micelles (such as SDS and CTAB), where the headgroups are loosely packed because of charge repulsions [28]. A small part of the increase in fluorescence polarization may be attributed to the increase in the size of the SDS micelles (which decreases the rate of rotation of the micelle) with increasing salt concentrations [20].

The fluorescence polarization of micelle-bound NBD-cholesterol, on the other hand, was found to decrease with increasing salt concentrations. However, a small increase in polarization was observed at a high salt concentration (see Fig. 7). This is in contrast to an earlier observation that upon sphere-to-rod transition, the

microviscosity in the micellar interior is increased [34]. The decrease in polarization upon salt addition could be interpreted as arising due to a change in probe localization brought about by the structural transition. Deeper localization of probes resulting from sphere-to-rod transition has been reported [33]. This is further supported by accessibility studies done with Co^{2+} as a quencher of NBD fluorescence. The small increase in polarization observed at high salt concentrations could indicate tighter packing at high NaCl concentrations.

Accessibility Studies of Micelle-Bound Fluorophores

To examine the relative locations of the NBD probes in various types of micelles, fluorescence quenching experiments were performed with the aqueous quencher Co^{2+}. The paramagnetic cobaltous ion is soluble in water and has been shown to be an efficient quencher of NBD fluorescence [62,82,83]. The results of these experiments for NBD-PE and NBD-cholesterol are plotted in Figs. 8 and 9, respectively, as Stern–Volmer plots. The slope of such a plot is related to the degree of exposure of the NBD group to the aqueous phase. In general, the higher the slope, the greater the degree of exposure, assuming that there is not a large difference in fluorescence lifetime. On this basis, it is apparent from Figs. 8 and 9 that the NBD group in NBD-PE (Fig. 8) or NBD-cholesterol (Fig. 9) is the most exposed (most shallow) in the absence of NaCl, *i.e.*, in spherical micelles of SDS. Among these two probes, the fluorescence of NBD-PE is quenched to a much greater extent at a lower Co^{2+} concentration than observed with NBD-cholesterol. This is indicative of an interfacial (shallow) location of the NBD group in micelle-bound NBD-PE, as opposed to the rather deep localization of the NBD group in micelle-bound NBD-cholesterol. The Stern–Volmer plots in Figs. 8 and 9 display deviations from linearity. The deviation is toward the ordinate (y-axis) in Fig. 8 in the absence of NaCl. This could imply a contribution from static quenching. In Fig. 9, however, the deviation is toward the abscissa (x-axis), especially when NaCl is absent. This could be due to heterogeneity in probe location.

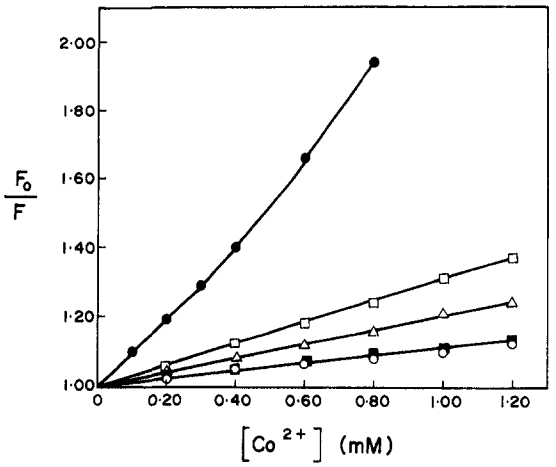

Fig. 8. Stern–Volmer plot of NBD-PE fluorescence in SDS micelles by Co^{2+} in the absence (●) and in the presence of 0.1 *M* (□), 0.2 *M* (△), and 0.5 *M* (○) NaCl. F_0 is the fluorescence in the absence of quencher and F is the fluorescence in the presence of quencher. The ratio of NBD-PE to SDS was 1:10,000 (mol/mol). Also shown is the plot of NBD-PE quenching in DOPC vesicles (■). The NBD-PE-to-DOPC ratio was 1:100 (mol/mol) in vesicles. The excitation wavelength was fixed at 465 nm for all experiments and emission was monitored at 530 nm. See Experimental for other details.

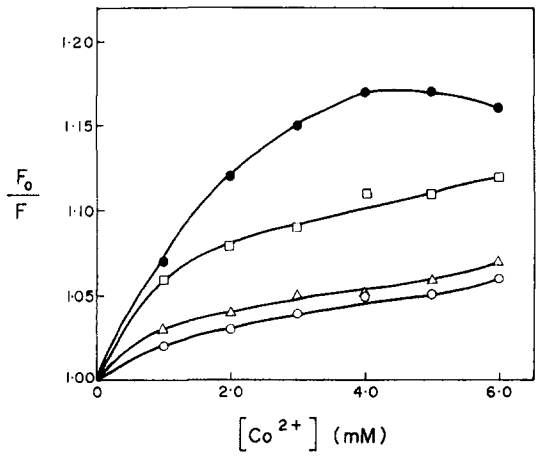

Fig. 9. Stern–Volmer plot of NBD-cholesterol fluorescence in SDS micelles by Co^{2+} in the absence of NaCl (●) and in the presence of 0.1 *M* (□) and 0.5 *M* (△) NaCl. F_0 is the fluorescence in the absence of quencher and F is the fluorescence in the presence of quencher. The ratio of NBD-cholesterol to SDS was 1:10,000 (mol/mol). Also shown is the plot of NBD-cholesterol quenching in DOPC vesicles (○). The NBD-cholesterol-to-DOPC ratio was 1:100 (mol/mol) in vesicles. The excitation wavelength was fixed at 465 nm for all experiments and emission was monitored at 527 nm. See Experimental for other details.

The accessibilities of the NBD groups change in both cases upon the addition of NaCl when rod-shaped micelles begin to appear. In both cases, the NBD group appears deeper (*i.e.*, the slope of the Stern–Volmer plot is lowered) when 0.1 *M* NaCl is present in the medium. This is indicative of a deeper localization of the probes induced by shape change in the micellar assembly. This also points out the differences in packing in these two types of micelles, with rod-shaped micelles having a tighter packing arrangement and hence being less accessible to the aqueous quencher. This is supported by fluorescence polarization results (see above). The accessibility profiles (Stern–Volmer plots) in the presence of 0.1 and

0.2 *M* NaCl indicate intermediates in sphere-to-rod shape transition. Upon increasing the NaCl concentration to 0.2 *M* and then, finally, to 0.5 *M*, there is further lowering of the Stern–Volmer slope. Thus, the accessibilities of both the fluorophores were found to decrease as the ionic strength of the medium was increased. Interestingly, in the presence of 0.5 *M* NaCl, the Stern–Volmer plots for micelle-bound NBD-PE and NBD-cholesterol were found to overlap with that of membrane (bilayer)-bound NBD-PE and NBD-cholesterol. The rod-shaped micelles have been proposed to have an organization of amphiphiles similar to that of a bilayer [34]. These results are in agreement with this proposal.

Changes in Fluorescence Lifetime as a Function of NaCl Concentration

Since fluorescence lifetime serves as a sensitive indicator of the local environment in which a given fluorophore is placed, any change in the microenvironment of a micelle-bound probe could be expected to give rise to differences in its lifetime. All fluorescence decays for micelle-bound NBD-PE could be fitted well with a biexponential function (see Table I). As can be seen from Table I, when micelle-bound NBD-PE is excited at 337 nm, the decay fits a biexponential function, with a relatively short lifetime component (~1.0 ns) and a longer lifetime component (around 3.0 ns). A typical decay profile with its biexponential fitting and the various statistical parameters used to check the goodness of the fit is shown in Fig. 10.

Table I shows the lifetimes of NBD-PE in SDS micelles as a function of NaCl concentration. In order to obtain a comprehensive picture of these lifetime changes, the same set of fluorescence decays was subjected to global analysis. The decays were all assumed to be biexponential (on the basis of the results from discrete analysis), with lifetime components that were assumed to be linked among the data files and whose relative contributions (preexponential factors) were allowed to vary. The

Table I. Lifetimes of NBD-PE as a Function of NaCl Concentration[a]

[NaCl] (*M*)	α_1	τ_1 (ns)	α_2	τ_2 (ns)
0	0.38 (0.81)[b]	1.39 (2.26)	0.62 (0.19)	3.05 (3.92)
0.1	0.34 (0.61)	0.96 (2.26)	0.66 (0.39)	3.31 (3.92)
0.2	0.37 (0.54)	0.96 (2.26)	0.63 (0.46)	3.46 (3.92)
0.5	0.48 (0.45)	0.70 (2.26)	0.52 (0.55)	3.61 (3.92)

[a] Excitation wavelength, 337 nm; emission wavelength, 531 nm.
[b] Numbers in parentheses are the results of global analysis.

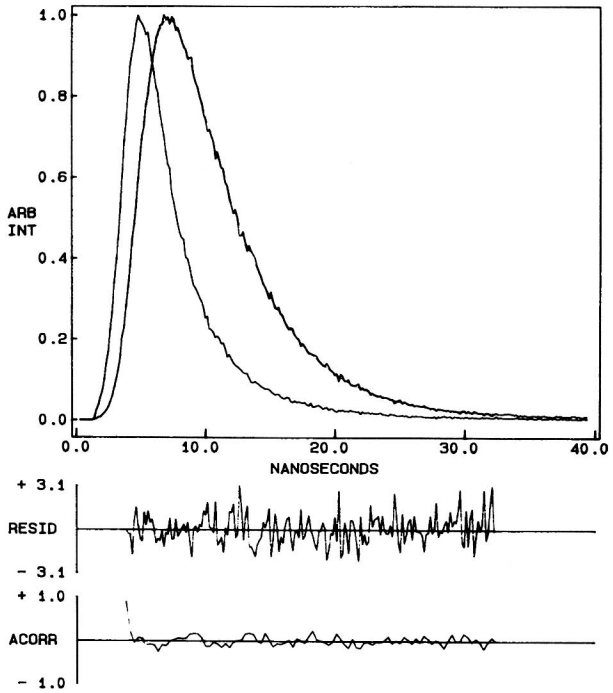

Fig. 10. Time-resolved fluorescence intensity decay of NBD-PE in SDS micelles containing 0.1 *M* NaCl when excited at 337 nm, which corresponds to a peak in the spectral output of the nitrogen flash lamp. Emission wavelength was monitored at 531 nm. The sharp peak at the left is the lamp profile. The relatively broad peak at the right is the decay profile, fitted to a biexponential function. The two lower plots show the weighted residuals and the autocorrelation function of the weighted residuals. The ratio of NBD-PE to SDS was 1:10,000 (mol/mol). See Experimental for other details.

results of the global analysis are shown in parentheses in Table I. The fittings of the set of decay profiles analyzed by the global method are presented as a pseudo-three-dimensional plot of intensity *vs* time *vs* increasing file number in Fig. 11a. The weighted residuals corresponding to each of these fittings are also shown (Fig. 11b). The normalized global χ^2 value obtained was 1.19.

The mean fluorescence lifetimes of micelle-bound NBD-PE were calculated using Eq. (4) and are plotted as a function of NaCl concentration in Fig. 12 for both discrete and global analysis. As shown in this figure, there is a steady increase in the mean lifetimes of NBD-PE with increasing NaCl concentration, irrespective of the method of analysis (discrete or global). Such a marked increase in the mean fluorescence lifetime as a function of the NaCl concentration is indicative of changes in the microenvironment of micelle-bound NBD-PE. This could be due to a change in the polarity and/or a change in the location of the probe molecule in the micellar assembly. The fluorescence lifetime of the NBD group is known to decrease in the presence of polar solvents such as water.

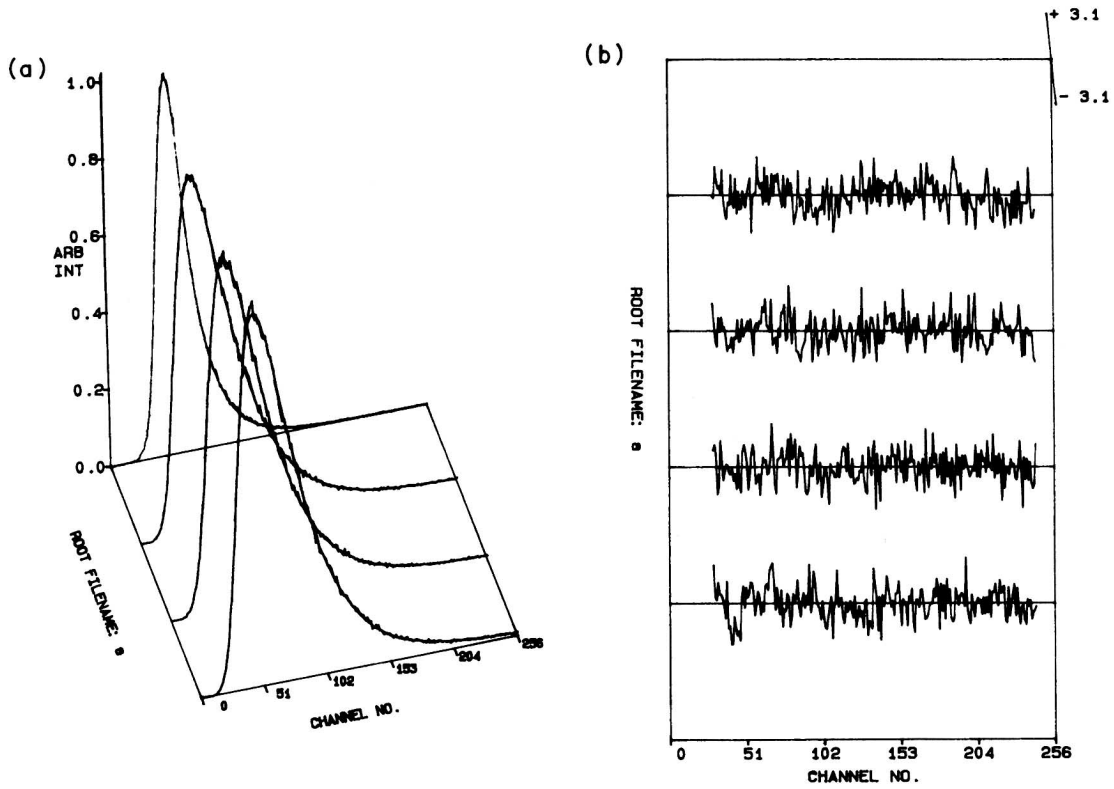

Fig. 11. Global fittings and corresponding weighted residuals of the set of decay profiles of NBD-PE in SDS micelles obtained as a function of increasing salt concentrations (0–0.5 *M* NaCl). The ratio of NBD-PE to SDS was 1:10,000 (mol/mol). See Experimental for other details.

Thus, while the lifetime of NBD-PE in membranes has been reported to be 6–8 ns [45,84], it reduces to ~1.5 ns in water due to hydrogen bonding interactions between the NBD group and the solvent [80], which are accompanied by an increase in the rate of nonradiative decay [60]. The geometry and packing features of spherical micelles are somewhat loose [29], allowing more water penetration into the micellar interior [18]. The increase in the lifetime of micelle-bound NBD-PE with increasing NaCl concentrations could thus reflect the changes in the water content of the micelles accompanying the shape transition from spherical to rod-shaped micelles, the lifetime being longer in micelles with a lower water content. Alternatively, as the fluorescence quenching experiments with Co^{2+} show, the location of NBD-PE undergoes a change with increasing NaCl concentrations (see Fig. 8). The changes in lifetime could be due to the deeper localization of NBD-PE in rod-shaped micelles.

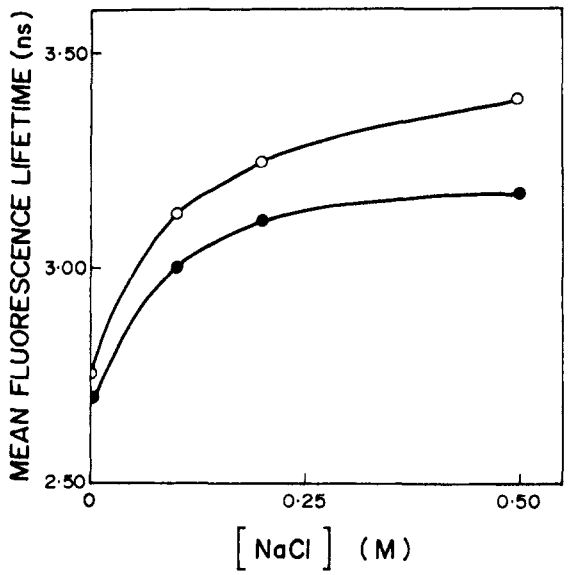

Fig. 12. Mean fluorescence lifetime of NBD-PE in SDS micelles as a function of NaCl concentration obtained by (•) discrete analysis and (○) global analysis. The emission wavelength was kept constant at 531 nm. Mean lifetimes were calculated from Table I using Eq. (4). The ratio of NBD-PE to SDS was 1:10,000 (mol/mol). See Experimental for other details.

DISCUSSION

Structural transitions involving shape changes play an important role in cellular physiology. For example,

the shape of erythrocytes (red blood cells) has recently been shown to change with the pH and ionic strength of the medium [85]. The shape of the erythrocyte (red blood cell) is thought to be maintained by the membrane skeleton in close interaction with the plasma membrane [86]. Investigations into the role of the membrane in such shape changes have revealed that modification of either the membrane composition or the structure of its individual constituents can lead to shape changes [87]. Thus, alteration of the cholesterol composition, selective removal of phospholipids from the outer membrane leaflet, pH and membrane potential alterations, metabolic depletion, and introduction of lysophospholipids, fatty acids, and charged amphipathic agents in membranes lead to shape changes in erythrocytes [87–89]. Shape changes can be induced even in liposomes by mechanical stress, temperature or pH variation, osmotic shock, and an asymmetric transmembrane distribution of phospholipids [90].

In this paper, we have examined shape changes associated with the salt-induced sphere-to-rod structural transition in charged micellar assemblies by monitoring changes in fluorescence of micelle-bound NBD probes. The NBD group possesses some of the most desirable properties for serving as an excellent probe for both spectroscopic and microscopic applications [67]. It is very weakly fluorescent in water. Upon transfer to a hydrophobic medium, it fluoresces brightly in the visible range and shows a high degree of environmental sensitivity [48,62,80,81,91]. This high degree of environmental sensitivity of NBD fluorescence can prove to be very useful in probing different types of micellar organizations formed by various detergents.

We have shown previously that wavelength-selective fluorescence represents a novel and convenient approach to monitoring micellar organization and dynamics [28]. In the present work, we have characterized the change in organization and dynamics accompanied by the salt-induced sphere-to-rod transition in SDS micelles using wavelength-selective fluorescence and steady-state and time-resolved fluorescence parameters of two micelle-bound NBD probes which are differentially localized in the micellar assembly. Our present results show that wavelength-selective fluorescence, in combination with other fluorescence parameters, offers a powerful way to monitor structural transitions induced in charged micelles. These results could be significant to changes in membrane morphology observed under certain physiological conditions.

ACKNOWLEDGMENTS

We thank Y. S. S. V. Prasad and G. G. Kingi for technical help and Dr. Sushmita Mukherjee for help during initial stages of this work. This work was supported by the Council of Scientific and Industrial Research, Government of India. S.S.R. thanks the Council of Scientific & Industrial Research for the award of a Senior Research Fellowship.

REFERENCES

1. A. Helenius and K. Simons (1975) *Biochim. Biophys. Acta* **415**, 29–79.
2. A. Helenius, D. R. McCaslin, E. Fries, and C. Tanford (1979) *Methods Enzymol.* **56**, 734–749.
3. L. M. Hjelmeland (1980) *Proc. Natl. Acad. Sci. USA* **77**, 6368–6370.
4. D. Lichtenberg, R. J. Robson, and E. A. Dennis (1983) *Biochim. Biophys. Acta* **737**, 285–304.
5. J. M. Neugebauer (1990) *Methods Enzymol.* **182**, 239–253.
6. A. Chattopadhyay and K. G. Harikumar (1996) *FEBS Lett.* **391**, 199–202.
7. C. Tanford (1978) *Science* **200**, 1012–1018.
8. J. N. Israelachvili, S. Marcelja, and R. G. Horn (1980) *Q. Rev. Biophys.* **13**, 121–200.
9. C. Tanford (1980) *The Hydrophobic Effect: Formation of Micelles and Biological Membranes*, Wiley–Interscience, New York.
10. C. Tanford (1987) *Biochem. Soc. Trans.* **15**, 1S–7S.
11. J. C. Franklin, J. F. Ellena, S. Jayasinghe, L. P. Kelsh, and D. S. Cafiso (1994) *Biochemistry* **33**, 4036–4045.
12. S. Improta, A. Pastore, S. Mammi, and E. Peggion (1994) *Biopolymers* **34**, 773–782.
13. V. J. Lenz, M. Federwisch, H.-G. Gattner, D. Brandenburg, H. Hocker, U. Hassiepen, and A. Wollner (1995) *Biochemistry* **34**, 6130–6141.
14. G. L. Mattice, R. E. Koeppe, L. L. Providence, and O. S. Andersen (1995) *Biochemistry* **34**, 6827–6837.
15. N. A. Mazer, G. B. Benedek, and M. C. Carey (1976) *J. Phys. Chem.* **80**, 1075–1086.
16. C. Y. Young, P. J. Missel, N. A. Mazer, G. B. Benedek, and M. C. Carey (1978) *J. Phys. Chem.* **82**, 1375–1378.
17. S. Hayashi and S. Ikeda (1980) *J. Phys. Chem.* **84**, 744–751.
18. F. M. Menger (1979) *Acc. Chem. Res.* **12**, 111–117.
19. B. Lindman and H. Wennerstrom (1982) in K. L. Mittal and E. J. Fendler (Eds.), *Solution Behavior of Surfactants: Theoretical and Applied Aspects*, Plenum Press, New York, Vol. 1, pp. 3–25.
20. M. Shinitzky, A.-C. Dianoux, C. Gitler, and G. Weber (1971) *Biochemistry* **10**, 2106–2113.
21. K. Kalyanasundaram and J. K. Thomas (1977) *J. Phys. Chem.* **81**, 2176–2180.
22. P. Mukerjee and J. R. Cardinal (1978) *J. Phys. Chem.* **82**, 1620–1627.
23. R. Leung and D. O. Shah (1986) *J. Colloid Interface Sci.* **113**, 484–499.
24. H. Nery, O. Soderman, D. Canet, H. Walderhaug, and B. Lindman (1986) *J. Phys. Chem.* **90**, 5802–5808.
25. G. Saroja and A. Samanta (1995) *Chem. Phys. Lett.* **246**, 506–512.
26. N. Sarkar, A. Datta, S. Das, and K. Bhattacharyya (1996) *J. Phys. Chem.* **100**, 15483–15486.
27. N. C. Maiti, M. M. G. Krishna, P. J. Britto, and N. Periasamy (1997) *J. Phys. Chem. B* **101**, 11051–11060.
28. S. S. Rawat, S. Mukherjee, and A. Chattopadhyay (1997) *J. Phys. Chem. B* **101**, 1922–1929.
29. D. W. R. Gruen (1985) *J. Phys. Chem.* **89**, 153–163.
30. A. D. MacKerell (1995) *J. Phys. Chem.* **99**, 1846–1855.
31. K. N. Ganesh, P. Mitra, and D. Balasubramanian (1982) *J. Phys. Chem.* **86**, 4291–4293.
32. J. Shobha and D. Balasubramanian (1986) *J. Phys. Chem.* **90**, 2800–2802.
33. J. Shobha, V. Srinivas, and D. Balasubramanian (1989) *J. Phys. Chem.* **93**, 17–20.

34. K. Kalyanasundaram, M. Gratzel, and J. K. Thomas (1975) *J. Am. Chem. Soc.* **97**, 3915–3922.
35. S. Ikeda, S. Hayashi, and T. Imae (1981) *J. Phys. Chem.* **85**, 106–112.
36. P. J. Missel, N. A. Mazer, M. C. Carey, and G. B. Benedek (1982) in K. L. Mittal and E. J. Fendler (Eds.), *Solution Behavior of Surfactants: Theoretical and Applied Aspects*, Plenum Press, New York, Vol. 1, pp. 373–388.
37. S. Ikeda (1984) in K. L. Mittal and E. J. Fendler (Eds.), *Surfactants in Solution*, Plenum Press, New York, Vol. 2, pp. 825–840.
38. G. Porte and J. Appell (1984) in K. L. Mittal and E. J. Fendler (Eds.), *Surfactants in Solution*, Plenum Press, New York, Vol. 2, pp. 805–823.
39. P. Mukerjee (1965) *J. Phys. Chem.* **69**, 4038–4040.
40. J. A. Reynolds and C. Tanford (1970) *Proc. Natl. Acad. Sci. USA* **66**, 1002–1007.
41. A. Chattopadhyay and E. London (1984) *Anal. Biochem.* **139**, 408–412.
42. K. Kalyanasundaram and J. K. Thomas (1976) *J. Phys. Chem.* **80**, 1462–1473.
43. J. Shobha and D. Balasubramanian (1987) *Proc. Indian Acad. Sci. (Chem. Sci.)* **98**, 469–478.
44. A. Chattopadhyay (1991) *Biophys. J.* **59**, 191a.
45. A. Chattopadhyay and S. Mukherjee (1993) *Biochemistry* **32**, 3804–3811.
46. A. Chattopadhyay and R. Rukmini (1993) *FEBS Lett.* **335**, 341–344.
47. S. Mukherjee and A. Chattopadhyay (1994) *Biochemistry* **33**, 5089–5097.
48. S. Mukherjee, A. Chattopadhyay, A. Samanta, and T. Soujanya (1994) *J. Phys. Chem.* **98**, 2809–2812.
49. S. Guha, S. S. Rawat, A. Chattopadhyay, and B. Bhattacharyya (1996) *Biochemistry* **35**, 13426–13433.
50. A. Chattopadhyay, S. Mukherjee, R. Rukmini, S. S. Rawat, and S. Sudha (1997) *Biophys. J.* **73**, 839–849.
51. A. K. Ghosh, R. Rukmini, and A. Chattopadhyay (1997) *Biochemistry* **36**, 14291–14305.
52. S. Mukherjee and A. Chattopadhyay (1995) *J. Fluoresc.* **5**, 237–246.
53. A. P. Demchenko (1988) *Trends Biochem. Sci.* **13**, 374–377.
54. D. Haussinger (1996) *Biochem. J.* **313**, 697–710.
55. C. Ho and C. D. Stubbs (1992) *Biophys. J.* **63**, 897–902.
56. W. B. Fischer, S. Sonar, T. Marti, H. G. Khorana, and K. J. Rothschild (1994) *Biochemistry* **33**, 12757–12762.
57. H. Kandori, Y. Yamazaki, J. Sasaki, R. Needleman, J. K. Lanyi, and A. Maeda (1995) *J. Am. Chem. Soc.* **117**, 2118–2119.
58. R. Sankararamakrishnan and M. S. P. Sansom (1995) *FEBS Lett.* **377**, 377–382.
59. A. Chattopadhyay (1990) *Chem. Phys. Lipids* **53**, 1–15.
60. S. Mazeres, V. Schram, J.-F. Tocanne, and A. Lopez (1996) *Biophys. J.* **71**, 327–335.
61. A. Chattopadhyay and E. London (1987) *Biochemistry* **26**, 39–45.
62. A. Chattopadhyay and E. London (1988) *Biochim. Biophys. Acta* **938**, 24–34.
63. R. E. Pagano and O. C. Martin (1988) *Biochemistry* **27**, 4439–4445.
64. B. Mitra and G. G. Hammes (1990) *Biochemistry* **29**, 9879–9884.
65. D. E. Wolf, A. P. Winiski, A. E. Ting, K. M. Bocian, and R. E. Pagano (1992) *Biochemistry* **31**, 2865–2873.
66. F. S. Abrams and E. London (1993) *Biochemistry* **32**, 10826–10831.
67. S. Mukherjee and A. Chattopadhyay (1996) *Biochemistry* **35**, 1311–1322.
68. J. C. Dittmer and R. L. Lester (1964) *J. Lipid Res.* **5**, 126–127.
69. C. W. F. McClare (1971) *Anal. Biochem.* **39**, 527–530.
70. R. F. Chen and R. L. Bowman (1965) *Science* **147**, 729–732.
71. J. R. Lakowicz (1983) *Principles of Fluorescence Spectroscopy*, Plenum Press, New York.
72. P. R. Bevington (1969) *Data Reduction and Error Analysis for the Physical Sciences*, McGraw–Hill, New York.
73. D. V. O'Connor and D. Phillips (1984) *Time-Correlated Single Photon Counting*, Academic Press, London, pp. 180–189.
74. R. A. Lampert, L. A. Chewter, D. Phillips, D. V. O'Connor, A. J. Roberts, and S. R. Meech (1983) *Anal. Chem.* **55**, 68–73.
75. A. Grinvald and I. Z. Steinberg (1974) *Anal. Biochem.* **59**, 583–598.
76. J. R. Knutson, J. M. Beechem, and L. Brand (1983) *Chem. Phys. Lett.* **102**, 501–507.
77. J. M. Beechem (1989) *Chem. Phys. Lipids* **50**, 237–251.
78. J. M. Beechem (1992) *Methods Enzymol.* **210**, 37–54.
79. J. M. Beechem, E. Gratton, M. Ameloot, J. R. Knutson, and L. Brand (1991) in J. R. Lakowicz (Ed.), *Topics in Fluorescence Spectroscopy: Principles*, Plenum Press, New York, Vol. 2, pp. 241–305.
80. S. Lin and W. S. Struve (1991) *Photochem. Photobiol.* **54**, 361–365.
81. S. Fery-Forgues, J. P. Fayet, and A. Lopez (1993) *J. Photochem. Photobiol.* **70**, 229–243.
82. R. Homan and M. Eisenberg (1985) *Biochim. Biophys. Acta* **812**, 485–492.
83. S. J. Morris, D. Bradley, and R. Blumenthal (1985) *Biochim. Biophys. Acta* **818**, 365–372.
84. T. Arvinte, A. Cudd, and K. Hildenbrand (1986) *Biochim. Biophys. Acta* **860**, 215–228.
85. M. Rasia and A. Bollini (1998) *Biochim. Biophys. Acta* **1372**, 198–204.
86. E. J. Luna and A. L. Hitt (1992) *Science* **258**, 955–963.
87. F. A. Kuypers, B. Roelofsen, W. Berendsen, J. A. F. Op den Kamp, and L. L. M. van Deenen (1984) *J. Cell Biol.* **99**, 2260–2267.
88. L. Backman, J. B. Jonasson, and P. Horstedt (1998) *Mol. Membr. Biol.* **15**, 27–32.
89. M. M. Gedde and W. H. Huestis (1997) *Biophys. J.* **72**, 1220–1233.
90. E. Farge and P. F. Devaux (1992) *Biophys. J.* **61**, 347–357.
91. K. Rajarathnam, J. Hochman, M. Schindler, and S. Ferguson-Miller. (1989) *Biochemistry* **28**, 3168–3176.